Journal of Microscopy, Vol. 228, Pt 2 2007, pp. 132–138
Received 24 September 2006; accepted 18 May 2007

Three-dimensional point spread function model for line-scanning confocal microscope with high-aperture objective

E. DUSCH*,†, T. DORVAL*, N. VINCENT†, M. WACHSMUTH‡ & A. GENOVESIO*
Image Mining Group, Institut Pasteur Korea, 39-1, Halwolgok-dong, Seongbuk-gu, Seoul 136-791, Korea, †SIP-CRIP5, Université Paris Descartes, 45, rue des Saint Pères 75005 Paris, France and ‡Cell Biophysics Group, Institut Pasteur Korea, 39-1, Halwolgok-dong, Seongbuk-gu, Seoul 136-791, Korea

Key words. Confocal microscopy, Debye integral, line-scanning confocal microscope, point spread function.

Summary

Point Spread Function (PSF) modelling is an important task in image formation analysis. In confocal microscopy, the exact PSF is rarely known, thus one has to rely on its approximation. An initial estimation is usually performed experimentally by measuring fluorescent beads or analytically by studying properties of the optical system. Yet, fluorescent line-scanning confocal microscopes are not widespread; therefore, very few adapted models are available in the literature. In this paper, we propose an analytical PSF model for line-scanning confocal microscopes. Validation is performed by measuring the error between our model and an experimental PSF measured with fluorescent beads, assumed to represent the real PSF. Comparison with existing models is also presented.

Introduction

Accurate point spread function (PSF) models are necessary for various tasks, such as deconvolution (see Sarder & Nehorai, 2006 for a review), image resolution improvement (Santos & Young, 2000; Thomann *et al.*, 2002) and data simulation to validate image-processing algorithms. As the exact PSF is rarely known, one has to rely on its approximation, which can be estimated using an experimental or an analytical approach.

In an experimental approach, the PSF is estimated by extracting image structures assumed to represent it. In confocal microscopy, this is usually achieved by measuring small fluorescent beads. Although this approach has the advantage of well reflecting the imaging conditions, the obtained PSF has a low signal-to-noise ratio (SNR) due to the small size of the imaged beads (McNally *et al.*, 1999). Moreover, knowledge of both the analytical and the simulated PSF allows a more precise characterization of the system.

An analytical approach consists in expressing the PSF using diffraction theory and knowledge of the optical microscope components. Although analytical PSF models have been well established for point-scanning confocal microscopes, they are not adapted to line-scanning confocal microscopes (characterized by a line illumination in the object space and a slit-shaped line detector). In Sheppard & Mao (1988), the authors proposed a two-dimensional PSF model applicable only in the focal plane. More recently, Wolleschensky *et al.* (2005) proposed a three-dimensional (3D) model for the LSM 5 live line-scanning confocal microscope (Zeiss, Germany). They make a paraxial assumption, valid only for an objective lens with low numerical aperture (NA), and compute the model with non-paraxial optical units, which can be considered as a first approximation for higher NAs (Amos, 1995).

In this paper, we propose a 3D non-paraxial PSF model for a fluorescent line-scanning confocal microscope with a high-aperture objective lens, and show that the model tends asymptotically to the paraxial model of Wolleschensky *et al.*, when the NA becomes small. During the validation process, we use as reference a measured PSF calculated by averaging fluorescent beads imaged on the LSM 5 live microscope, and compare the relative absolute error (RAE) of three models: non-paraxial point-scanning (Gu, 2000), paraxial line-scanning (Wolleschensky *et al.*, 2005) and the proposed non-paraxial line-scanning model.

Theoretical line-scanning PSF model

In this section, we first express the theoretical excitation and emission amplitudes of a point near the focus using the scalar

Correspondence to: E. Dusch. Tel: +82 2 3299 0262; Fax: +82 2 3299 0210 e-mail: elodie.dusch@ip-korea.org; A. Genovesio. Tel: +82 2 3299 0261; Fax: +82 2 3299 0210; e-mail: agenoves@ip-korea.org

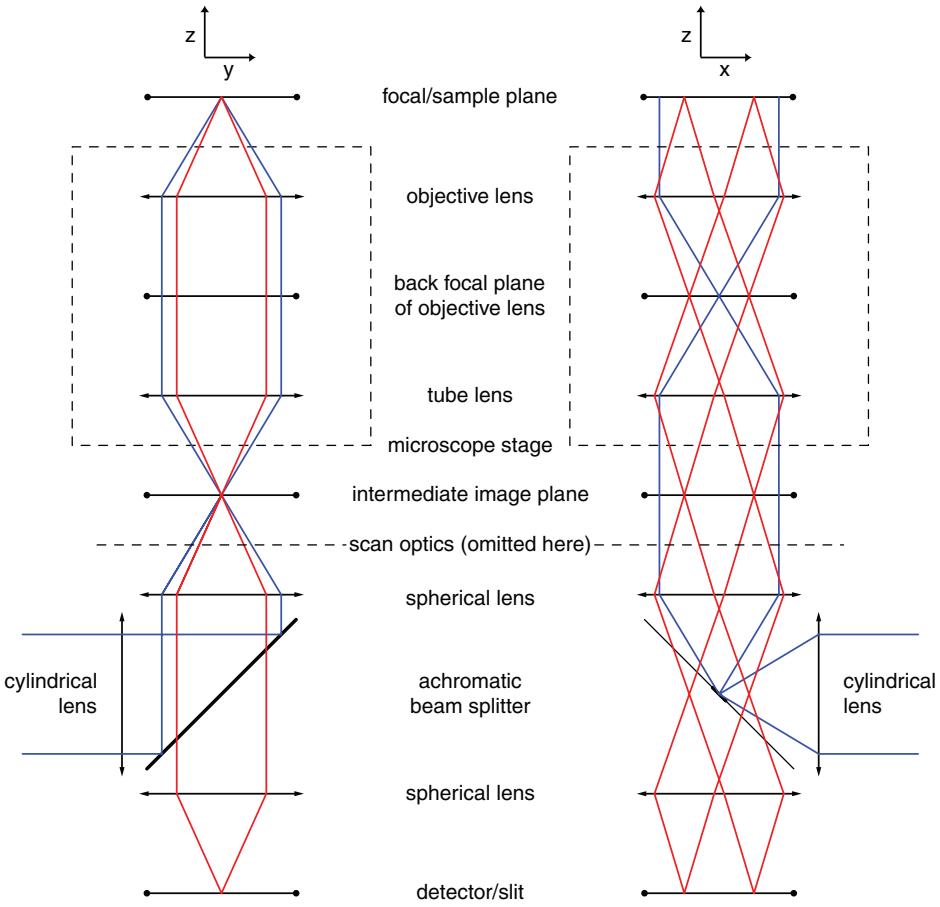

Fig. 1. Scheme of a fluorescent line-scanning confocal microscope.

Debye diffraction integral. Then, we present a 3D non-paraxial PSF model for fluorescent line-scanning confocal microscopes and its paraxial approximation.

When the NA becomes large, effects such as depolarization, apodization and aberration are more pronounced (Gu, 2000). Considering the vectorial property of electromagnetic waves, the vectorial Debye theory was proposed to take into account light depolarization in the focus of the lens. Nevertheless, a close approximation of the intensity distribution near the focus can be obtained by the scalar theory as shown by Born & Wolf (1999). In the following, we assume that the optical system is linear shift-invariant and aberration-free.

Let us consider a line illumination created and focussed by a cylindrical lens on the back-focal plane of the objective lens. A line is thus generated along the x direction by the objective lens onto the sample plane (Wolleschensky *et al.*, 2005).

Figure 1 describes the light path along the y direction (left) and x direction (right). The emitted fluorescence is focussed by the confocal lens onto a slit, rejecting out-of-focus fluorescent points.

In confocal microscopy, the Point Spread Function is defined by the product of the excitation intensity distribution (characterized by the line illumination) and the emission intensity distribution (generated by the fluorescence) convolved with the area of the detector projected into the object space:

$$\mathrm{PSF}(x, y, z) = |h_{\mathrm{ex}}(x, y, z)|^2 \left(|h_{\mathrm{em}}(x, y, z)|^2 * D(x, y)\right), \quad (1)$$

where $*$ denotes the convolution, D is the detector, and h_{ex} and h_{em} are the excitation and emission amplitude distributions, respectively. In line-scanning microscopes, the detector is characterized by the slit in the y direction and by the line CCD detector elements in the x direction. In the widefield case, it has been shown that the CCD elements are usually small enough to be neglected in the image formation process (van Kempen, 1999). In a similar way and as shown in Fig. 2, the PSF for line-scanning microscopes can be approximated by

$$\mathrm{PSF}(x, y, z) = |h_{\mathrm{ex}}(x, y, z)|^2 \left(|h_{\mathrm{em}}(x, y, z)|^2 * S(y)\right). \quad (2)$$

The slit S situated in front of the line detector is considered as a finite-size incoherent pinhole, that is, it detects the light intensity (Wilson, 1995).

Since an illumination line covers the total sample plane in the x direction, diffraction effects are not important owing to the wide illuminated area. Therefore, we assume the excitation amplitude along the line to be constant. The waves in the field between the objective lens and the focal plane are defined as

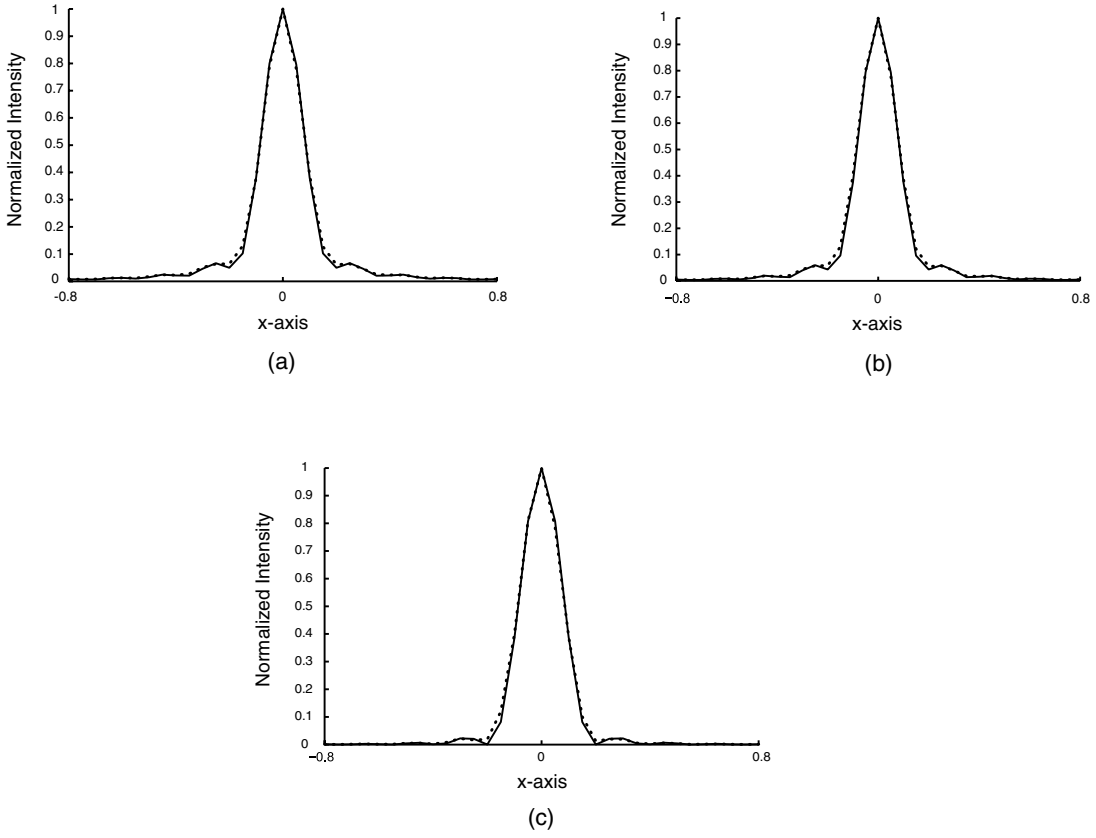

Fig. 2. Normalized intensity of the non-paraxial PSF model with (dashed line) and without (solid line) considering the detector along the line for different slit sizes: $s \to \infty$ (a), $s = 1$ (b) and $s \to 0$(c) (Units are in μm).

a superposition of plane waves. Using the scalar Debye theory (Born & Wolf, 1999), the excitation amplitude near the focal point can be written as the integration of these plane waves according to the angle of convergence. Thus, we express the excitation amplitude according to the y and z direction as (see Appendix A for details):

$$h_{\mathrm{ex}}(y, z) = \int_{-\alpha}^{\alpha} P(\theta) \exp(-ik_{\mathrm{ex}} y \sin\theta) \exp(-ik_{\mathrm{ex}} z \cos\theta)\, k_{\mathrm{ex}} \cos\theta d\theta, \quad (3)$$

where α is the aperture half angle of the objective and $k_{\mathrm{ex}} = n\frac{2\pi}{\lambda_{\mathrm{ex}}}$ is the excitation wave number. Under the sine condition, fulfilled by an aplanatic lens as generally used on commercial microscopes, the apodization term $P(\theta)$ is equal to $\sqrt{\cos\theta}$.

Similarly to a point-scanning confocal microscope, the emission amplitude distribution in front of the slit can be expressed by the scalar Debye diffraction integral for a circular lens:

$$h_{\mathrm{em}}(x, y, z) = \int_{0}^{\alpha} P(\theta) J_0(k_{\mathrm{em}} \sin\theta \sqrt{x^2 + y^2}) \times \exp(-ik_{\mathrm{em}} z \cos\theta)\, k_{\mathrm{em}} \sin\theta d\theta, \quad (4)$$

where the emission wave number k_{em} is equal to $n\frac{2\pi}{\lambda_{\mathrm{em}}}$, and J_0 is the zero-order Bessel function.

Hence, the non-paraxial line-scanning PSF can be written as

$$\mathrm{PSF}_{\mathrm{NP}}(x, y, z) = \int_{-s}^{s} \left| \int_{0}^{\alpha} \sqrt{\cos\theta} \exp(-ik_{\mathrm{ex}} y \sin\theta) \times \exp(-ik_{\mathrm{ex}} z \cos\theta) k_{\mathrm{ex}} \cos\theta d\theta \right|^2 \left| \int_{0}^{\alpha} \sqrt{\cos\theta} J_0\left(k_{\mathrm{em}} \sin\theta \sqrt{x^2 + (y - y_s)^2}\right) \times \exp(-ik_{\mathrm{em}} z \cos\theta)\, k_{\mathrm{em}} \sin\theta d\theta \right|^2 dy_s, \quad (5)$$

with s representing the half slit width in airy units. Figure 3 shows the normalized intensity PSF along each direction.

Approximation to low NAs

Equation (5) can be simplified for small NAs (inferior to 0.7). Under the assumptions ($\sin\theta \approx \theta$) and ($\cos\theta \approx \theta$), if we

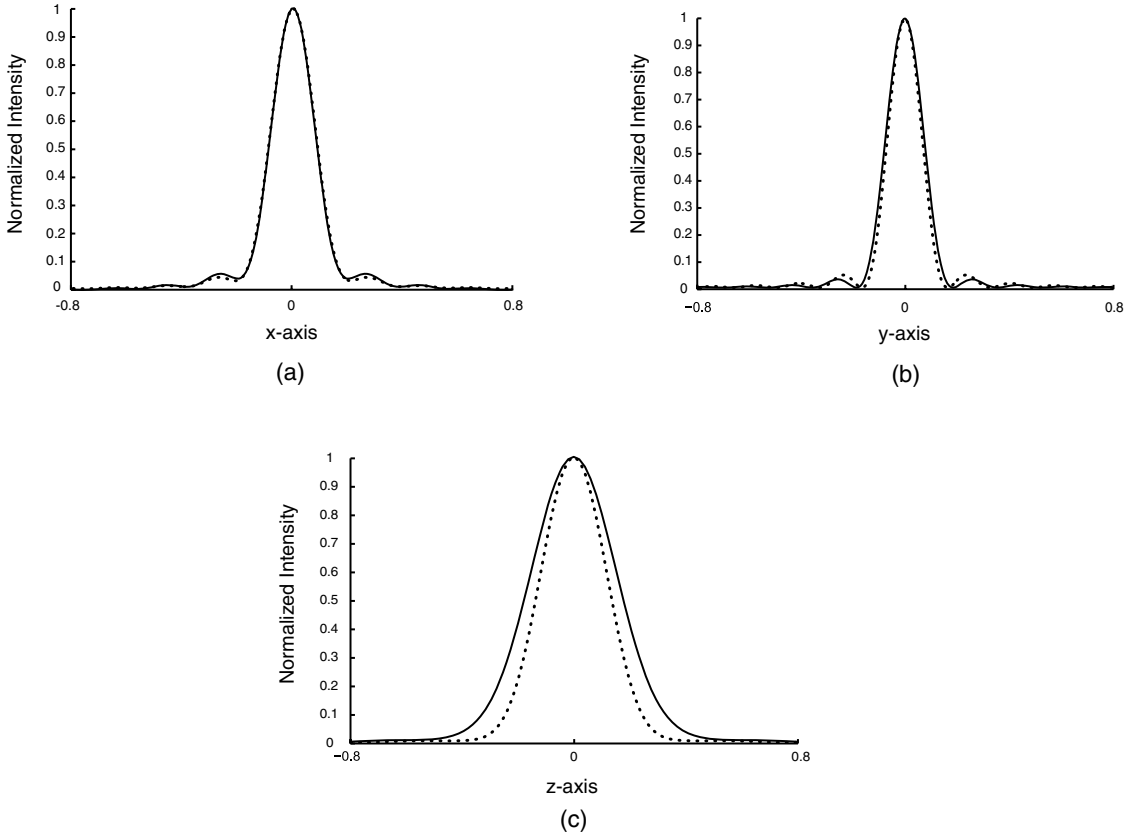

Fig. 3. Normalized intensity of the non-paraxial PSF model (Eq. 5, solid line) and of the paraxial PSF model (Eq. 6, dashed line) along the x (line) axis (a), the y(slit) axis (b) and the z(optical) axis (c) (units are in μm).

rewrite $\theta = \alpha t$, we find that Eq. (5) tends asymptotically to the following paraxial model:

$$\begin{aligned} \mathrm{PSF_P}(x, y, z) = & \left| \int_{-1}^{1} \exp\left(-ik_{\mathrm{ex}} y \alpha t\right) \right. \\ & \left. \times \exp\left(\frac{i}{2} k_{\mathrm{ex}} z \alpha^2 t^2\right) k_{\mathrm{ex}} dt \right|^2 \\ & \times \int_{-s}^{s} \left| \int_{0}^{1} J_0\left(k_{\mathrm{em}} \alpha t \sqrt{x + (y - y_s)^2}\right) \right. \\ & \left. \times \exp\left(\frac{i}{2} k_{\mathrm{em}} z \alpha^2 t^2\right) k_{\mathrm{em}} t dt \right|^2 dy_s, \end{aligned} \tag{6}$$

which is equivalent to the paraxial model given by Wolleschensky *et al.* (2005).

Validation

In this section, we compare our model with two other analytical models: non-paraxial point scanning (Gu, 2000) and paraxial line scanning (Wolleschensky *et al.*, 2005). We calculate an experimental PSF by measuring multiple PSF-like fluorescent beads, averaged to increase the SNR. The experimental PSF measurement is first presented, and then we compare the RAE between each model and the measured PSF.

Experimental PSF measurement

Material. Molecular Probes' PS-Speck beads used in our experiments are fluorescent spheres with a diameter of 0.175 μm (±0.005 μm). These fluorescent micro-spheres have an excitation and emission wavelength of 505 and 515 nm, respectively.

The beads were imaged on the LSM 5 live microscope with a resolution of 0.05 × 0.05 × 0.1 μm per voxel. We used a 488 nm/100 mW laser, a 505-nm emission long-pass filter and a 63× oil-immersion objective lens (NA = 1.4).

PSF-like structures extraction. We have developed a semi-automated method to extract the PSF-like fluorescent beads. Since the beads are randomly distributed over the sample, some may overlap and appear as clusters on the images. These clusters must be excluded from the measurement process; otherwise it yields an inaccurate PSF estimation. Therefore,

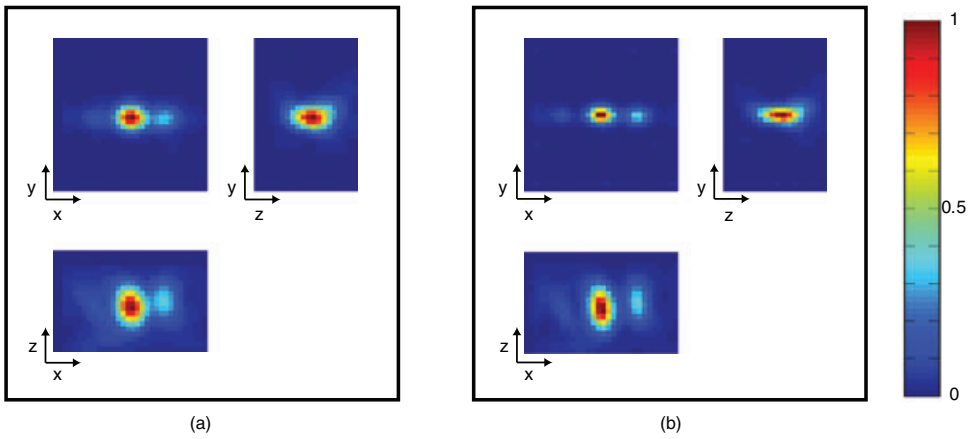

Fig. 4. *xy*, *xz* and *yz* views of the measured PSF before (a) and after (b) deconvolution. The measured PSF represents an average of more than 150 beads.

we define a criterion to discriminate background noise, isolated beads and bead clusters.

In the detection algorithm proposed by Thomann *et al.* (2002), the images are filtered with a Gaussian kernel of variance σ^2 that approximates the microscope's PSF, and a score is calculated for each local maximum as the product of the local average intensity and the Gaussian curvature κ (determinant of the Hessian matrix of the filtered image). This criterion is efficient to detect bright isotropic spots, but not adapted to our problem where the brightest structures are in fact bead clusters.

In our case, the Gaussian filtering is used to discriminate the size of the spots. The variance σ^2 affects the value of κ: a small σ^2 gives a high κ for small spots and low κ for large spots, and conversely, a large σ^2 gives a low κ for small spots and a high κ for large spots. For the background noise, intensity changes in all direction are randomly distributed, yielding a low κ. Thus, the Gaussian curvature is sufficient to discriminate each class. To extract the beads, the variance σ^2 is chosen to fit their size, and we apply a manual thresholding on the Gaussian curvature. κ Finally, isolated beads are cropped and averaged to get the measured PSF.

Beads averaging. To average the beads, we perform a sub-pixel accurate registration using the Polak-Ribiere method (Polak, 1971) to maximize the joint histogram mutual information (Viola & Wells, 1997). This criterion is widely used in the IRM field and is well suited for comparing images with different intensity ranges.

Bead image deconvolution. The experimental PSF measured using this protocol is larger than the analytical PSF model due to the beads' size. van der Voort & Strasters (1995) proposed to correct the blurring effect caused by the beads in estimating the experimental PSF by a deconvolution approach. Based on this work, we assume that the PSF was degraded by convolution with a virtual bead of diameter 0.175 μm under Poisson statistics, and we use the well-known iterative Richardson–Lucy algorithm to restore the experimental PSF. Original image and restored experimental PSF are presented in Fig. 4.

Results and discussion

To compare the analytical PSF models, we calculate the RAE with the experimental PSF:

$$\mathrm{RAE} = \frac{\sum_{i=1}^{n} |\mathrm{PSFM}_i - \mathrm{PSFA}_i|}{\sum_{i=1}^{n} \mathrm{PSFM}_i},$$

where PSFM and PSFA are, respectively, the measured and the analytical PSF, and n the number of pixels taken into consideration. Figure 5 shows the measured and simulated maximum centred PSFs along the *xy*, *xz* and *yz* view. Our model approximates the measured PSF with a RAE of 0.67 compared to 0.84 for the paraxial model and 0.95 for the point-scanning confocal model. Figure 6 shows the RAE along the axial direction, that is, computed plane by plane, between the measured and simulated PSFs. The RAE for the paraxial line-scanning model and the point-scanning model are always larger, showing that our model remains a better approximation everywhere along the *z* axis.

Despite the SNR increase by averaging fluorescent beads, the measured PSF is still corrupted by different sources of noises. Thus, the error could be reduced by including a noise model within the simulation process. Moreover, in the measured PSF, a divergent cone can be seen in the *xz* section (Fig. 5a). This phenomenon due to spherical aberrations is common in fluorescence microscopy. An additional aberration called coma can be seen in the *xy* section due to misalignment of the optical axis. We have assumed that the system is aberration-free, but taking these aberrations into account would

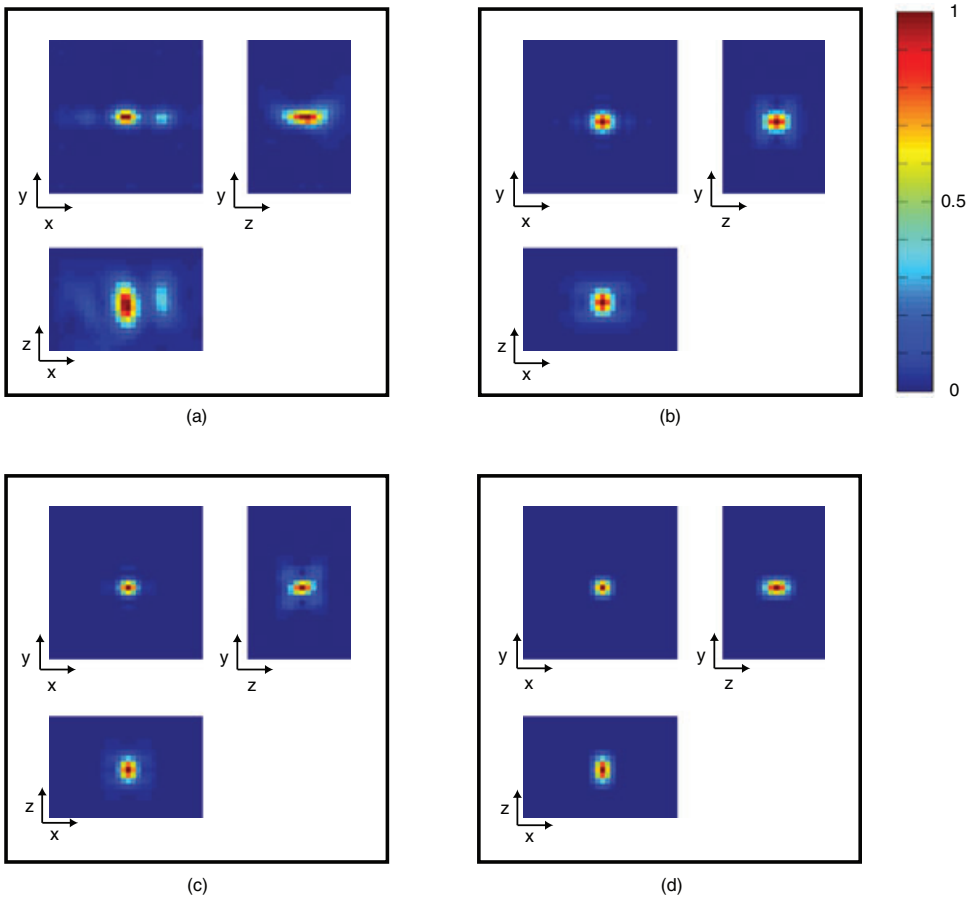

Fig. 5. *xy*, *xz* and *yz* views of the measured PSF (a), our non-paraxial model – RAE = 0.65 (b), paraxial line-scanning model – RAE = 0.84 (c) and point-scanning model – RAE = 0.95 (d).

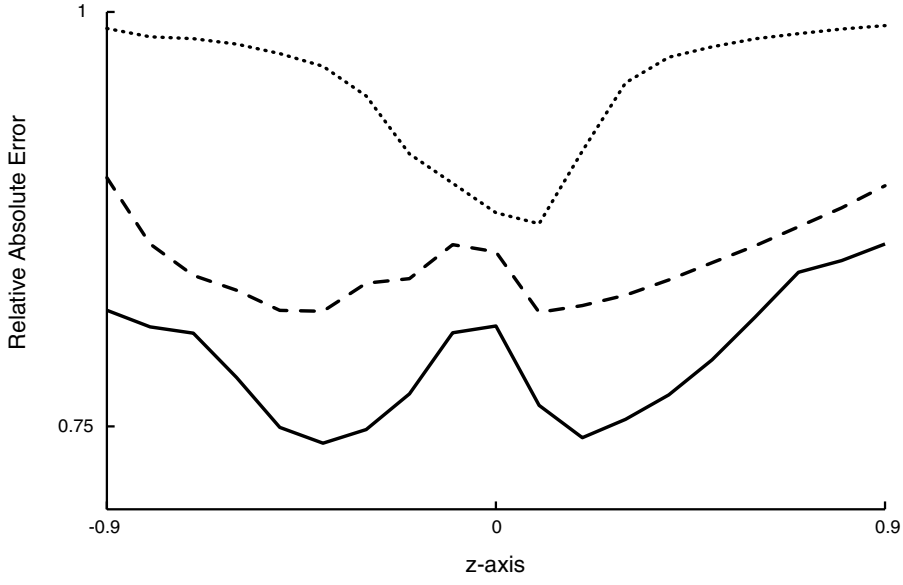

Fig. 6. RAE along the *z*-axis (in μm) between the measured PSF and the point-scanning model (point line), the paraxial line-scanning model (dashed line) and our non-paraxial model (solid line).

yield a much better PSF approximation, especially for high NAs.

Conclusion

We have presented an accurate PSF model for line-scanning confocal microscopes. A point-scanning confocal microscope PSF, a paraxial line-scanning confocal microscope PSF and our model were compared against an experimental PSF measured by averaging small fluorescent bead images. Our results show that our model substantially surpasses existing models. Still, it could be further improved by taking into account factors of disturbance such as depolarization and aberration (Török & Varga, 1997) and (Haeberlé *et al.*, 2003). In our future work, we will use this model in a deconvolution process to improve structure detection in several biological applications.

Acknowledgements

We thank Regis Grailhe and the Dynamic Imaging Platform of Institut Pasteur Korea for acquiring the beads images on the line-scanning confocal microscope. We also thank the reviewers for their constructive and detailed reviews of this manuscript.

References

Amos, W. (1995) Optical units. *Handbook of Biological Confocal Microscopy*, 2nd edn. (ed. by J. Pawley), pp. 579–580. Plenum Press, New York.

Born, M. & Wolf, E. (1999) *Principles of Optics*, 7th (expanded) edn. Pergamon, New York.

Gu, M. (2000) *Advanced Optical Imaging Theory*. Springer-Verlag, Berlin.

Haeberlé, O., Ammar, M., Furukawa, H., Tenjimbayashi, K. & Török, P. (2003) The point spread function of optical microscopes imaging through stratified media. *Opt. Exp.* **11**, 2964–2969.

van Kempen, G.M.P. (1999) *Image restoration in fluorescence microscopy*. PhD Thesis, Advanced School for Computing and Imaging.

McNally, J.G., Karpova, T., Cooper, J. & Conchello, J.A.L. (1999) Three dimensional imaging by deconvolution microscopy. *Methods* **19**, 373–385.

Polak, E. (1971) *Computational Methods in Optimization*. Academic Press, New York.

Santos, A. & Young, I.T. (2000) Model-based resolution: applying the theory in quantitative microscopy. *Appl. Opt.* **39**, 2948–2958.

Sarder, P. & Nehorai, A. (2006) Deconvolution methods for 3-D fluorescence microscopy images. *IEEE Sig. Proc. Mag.* **23**, 32–45.

Sheppard, C.J.R. & Mao, X.Q. (1988) Confocal microscopes with slit apertures. *J. Mod. Opt.* **35**, 1169–1185.

Thomann, D., Rines, D.R., Sorger, P.K. & Danuser, G. (2002) Automatic fluorescent tag detection in 3D with super-resolution: application to the analysis of chromosome movement. *J. Microsc.* **208**, 49–64.

Török, P. & Varga, P. (1997) Electromagnetic diffraction of light focused through a stratified medium. *Appl. Opt.* **39**, 2305–2312.

Viola, P. & Wells, W.M. (1997) Alignment by maximization of mutual information. *IJCV* **24**, 137–154.

van der Voort, H.T.M. & Strasters, K.C. (1995) Restoration of confocal images for quantitative image analysis. *J. Microsc.* **178**, 165–181.

Wilson, T. (1995) The role of the pinhole in confocal imaging system. *Handbook of Biological Confocal Microscopy*, 2nd edn. (ed. by J. Pawley), pp. 167–182. Plenum Press, New York.

Wolleschensky, R., Zimmermann, B., Ankerhold, R. & Kempe, M. (2005) High-speed scanning confocal microscope for the life sciences. *Confocal, Multiphoton, and Nonlinear Microscopic Imaging II. Proc. SPIE, vol. 5860* (ed. by T. Wilson), pp. 87–94.

Appendix: Excitation Amplitude

The scalar (or vectorial) Debye theory states that the amplitude (or electro-magnetic field) of a point near the focus can be expressed as a superposition of plane waves integrated on the lens aperture field A, leading to

$$h(y, z) = \int_A P(k_y, k_z) \exp(-i(k_y y + k_z z))dA,$$

where $P(k_y, k_z)$ is the pupil function (or the vectorial electromagnetic field distribution). This equation can also be seen as the Fourier transform of the pupil function. Using Fourier analysis, the PSF can be determined by the Fourier transform of the wavefront at the exit pupil plane. The wave vectors k_y and k_z can be described by the convergence angle θ of the pupil:

$$\begin{cases} k_y = k \sin\theta \\ k_z = k \cos\theta \end{cases}.$$

Under these transformations, the integration field dA and the pupil function are given by

$$dA = k \cos\theta d\theta$$
$$P(k_x, k_y) = P(\theta).$$

Finally, the integration is performed in the limit of the maximal angle of convergence α. The excitation amplitude becomes

$$h(y, z) = \int_{-\alpha}^{\alpha} P(\theta) \exp(-iky \sin\theta) \exp(-ikz \cos\theta) k \cos\theta d\theta.$$